Mixing Analysis of Combined Aeroramp/Strut Injectors in Supersonic Flow

Nikhil Hemanth, Amit Thakur, Corin Segal, Abhay Hervatte, and K. V. Shreyas

Abstract Scramjet engine is the most promising air breathing propulsion system in the hypersonic flight regime. Combustion in a scramjet engine, however, is difficult to achieve due to flow residence times being comparable to chemical times. For our study, 3-D RANS CFD analysis of a strut flame holder of a scramjet engine combustor was carried out. The first part of the analysis focuses on the validation of CFD gas dynamics results with earlier experimental data in literature. The air enters the combustor at Mach 2 with a stagnation temperature of 612 K and a stagnation pressure of 7.82 atm. Various flow properties like velocity profile, wall static pressure and density gradient were in good agreement with experimental results. The next part of the analysis involves a strut mounted across the walls of the combustor with hydrogen fuel injector jets forming an aerodynamic ramp on both the upper and lower surfaces. The location of the injectors relative to the strut base and dynamic pressure ratio were varied and the observations presented.

Keywords Scramjet · Aeroramp injector · Strut

1 Introduction

There has been extensive research carried out since the 1960s to fully understand and efficiently implement fuel injection and mixing in hypersonic flow. Ramp, step and struts have been extensively used for flame holding along with other physically intrusive techniques to promote fuel air mixing. Extensive numerical and experimental investigations have been performed with the strut flame holder spanning the length of the combustor. One such investigation performed at Georgia Tech involved fuel injection from the base of the strut and validation of numerical code with experiments at

N. Hemanth · C. Segal
University of Florida, Gainesville, FL, USA

A. Thakur (✉) · A. Hervatte · K. V. Shreyas
PES University, Bangalore, KA, India
e-mail: amit.thakur.amt@gmail.com

DLR wind tunnel facility in Germany [1]. Other Large Eddy Simulation (LES) studies have also been performed on the same configuration [2, 3]. Besides non-reacting flow, they also performed combustion analysis and enhanced the understanding of reacting flow beyond the available experimental data.

According to Fuller [4], a physically intrusive structure in supersonic flow will necessarily create hot spots, with thermal loads at specific locations exceeding the temperature limits of practical materials. Also, there are added problems of drag and loss in thrust with such physically intrusive structures [5]. In order to prevent the drawbacks of physically intrusive structures, Cox et al. [6] came up with a novel injector concept called the 'Aerodynamic ramp' or simply 'Aeroramp'. This injection technique initially involved a three by three array of closely spaced flush walled jets with a yaw angle given to each row. The objective was to create individual fuel vortices as a result of interaction between the skewed injection of one hole with that of the downstream hole. These individual fuel vortices are called skew induced vortices and along with shock induced vortex generation enhance mixing significantly [4].

Due to the absence of physically intrusive structures in the supersonic flow, hot spots and hence high thermal loading at specific locations is avoided. There is also lower associated stagnation pressure loss with this injection technique. Results of both numerical and experimental analysis performed by Fuller at the US Airforce research laboratory show that the Aeroramp injection technique achieved better mixing in the near field as compared to a physical ramp, increasing the jet-air momentum ratio enhanced the mixing performance in both the near as well as the far field. The total pressure loss incurred by the Aeroramp in all the cases was found to be lower than that of the physical ramp. It was also found that the total pressure loss decreased with increasing momentum ratio. Once the Aeroramp injection configuration proved to be a viable alternative to fuel injection in supersonic flow, several studies were performed to optimize it. This optimization was done to establish the parameters in terms of number, size, orientation and spacing of the Aeroramp holes.

Improvement to the design was done experimentally in Virginia Tech supersonic wind tunnel [7]. The study was a comparison of the mixing performance of a four flush walled hole Aeroramp injector with a single, low downstream angled hole in a cross-stream flow of Mach 2.4. It was found that eliminating the centre row of holes from the original nine flush walled holes and increasing the toe-in angle enhanced axial vortex formation. This axial vortex prevented the development of a secondary fuel core near the wall by lifting the entire plume off the wall, thus eliminating the possibility of hot spots at locations on the wall during reactive flow. Concurrently, studies were also performed to determine suitable toe-in angles and jet to freestream momentum flux ratios for injection [8]. It was found that increased momentum ratio improved core penetration of the fuel plume into the freestream. However, it also results in the formation of stronger bow shocks, leading to higher stagnation pressure loss. Increasing the toe-in angle increased the injected plume area but decreased its penetration into the freestream [4]. From the studies by Jacobsen, it was found that the 15° toe-in angle array with 30° transverse injection resulted in a minimised overall total pressure loss associated with the injector shock structure [8].

The toe-in angle is defined as the angle formed by the axis passing through the centre of the hole on the streamwise plane with the freestream. In the two row holes of the Improved Aerodynamic ramp study [7], this was taken as 15° for the front row and 30° for the rear row. The transverse injection angle is the angle at which the fuel is injected into a horizontally moving freestream. These angles are 20° and 40° respectively for the front and rear set of holes. The jet to freestream momentum flux ratio is defined as:

$$q = \frac{\left(\rho \times u^2\right)_j}{\left(\rho \times u^2\right)_\infty} = \frac{\left(\gamma \times P \times M^2\right)_j}{\left(\gamma \times P \times M^2\right)_\infty} \tag{1}$$

Combustion experiments with the Aeroramp were also performed with the integration of a plasma torch as a flame holder [9]. Dual mode ramjet combustion experiments with the Aeroramp configuration have shown this method of injection to be viable of mixing and stable combustion [10]. The idea was further evolved at Beijing University where Aeroramp injector was scaled down, non-reacting and combustion experiments were performed. A jet of hot exhaust gases at 3000 K was injected downstream of the Aeroramp to serve as a flame holder [11], a more detailed analysis of the flow field was done using CFD [12].

In present study, the aero-ramp fuel injectors were mounted on the upper and lower surfaces of the strut to improve the transverse penetration and mixing of fuel and air. The interaction of aero-ramp vortices with the recirculation zone behind the strut and its influence on the mixing process was investigated for different conditions.

2   Numerical Methodology

2.1   Geometry

The injection technique in the current work consists of two components: a strut which acts as the flame holder and spans the entire width of the combustor, the Aeroramp injection configuration on the upper and lower faces of the strut.

2.1.1   Strut Without Aeroramp Injectors

The DLR model of combustor used for the current work was obtained from literature [1] and is shown in Fig. 1. It has a length of 340 mm, width of 40 mm and a height of 50 mm at the inlet. The strut mounted across the walls of the combustor has a half angle of 6°. A 3° diverging slope is applied on the top wall of combustor to compensate for the boundary layer growth and effect of heat release on slowing down of supersonic flow.
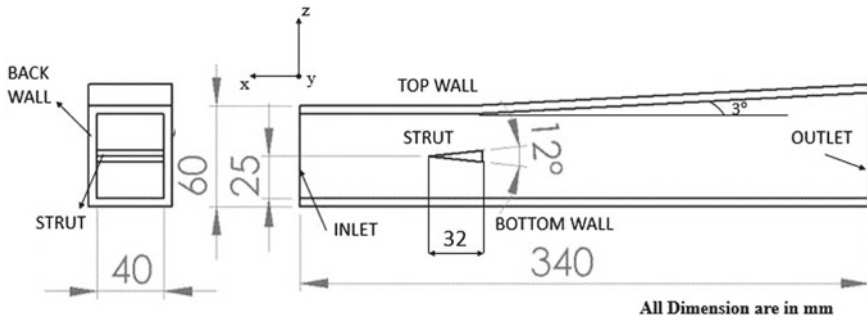
Fig. 1 Combustor geometry with strut flame holder

2.1.2   Strut with Aeroramp Injectors

The analysis deals with injecting fuel (H_2) from the top and bottom surfaces of the strut. In Fig. 2a, the isometric view of Aeroramp configuration on the upper face of the strut can be seen. An identical Aeroramp configuration is present on the lower face of the strut.

There are four injectors on the top surface and four on the bottom, making it a total of eight injectors. The injectors are placed in 2 rows. The front row of injectors is inclined at 29° with respect to the strut surface (35° with horizontal) and a toe-in angle of 20°. The back row of injectors is at a higher inclination of 49° with respect to the strut surface (55° with horizontal) and having a toe-in angle of 35°. The toe-in angles are indicated in Fig. 2b and transverse injection angles in Fig. 2c.

The location of Aeroramp injector with reference to the strut base was one of the parameters varied during the study, the end of the downstream injector row being 3 mm and 9 mm from the strut base respectively (Fig. 2b). When normalised with the length of the strut (32 mm), this corresponds to 0.09 and 0.28 for 3 mm and 9 mm from strut base respectively. Further increase in this distance would lead to a prohibitively small space for inclusion of the injector tubes. The holes have a jet diameter of 1 mm (d_j), with the equivalent diameter for four holes being 2 mm ($d_{eq} = 2d_j$). The front and back injectors were placed 8 mm ($4d_{eq}$) apart in the stream-wise direction with transverse spacing of 4 mm ($2d_{eq}$).

2.2   Mesh

A structured multi-block mesh was created using ICEM. The original mesh size was 3.4 million cells. The mesh was highly refined near the strut and combustor walls, giving y^+ less than 2, enough to capture the boundary layer gradients. The mesh was refined around the strut and its wake, with a cell size of approximately 0.2 mm and a moderate growth rate downstream of the strut. A finer mesh was obtained using
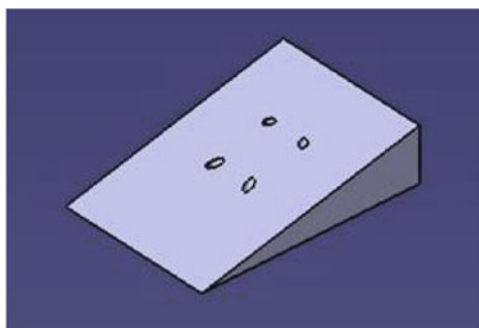
(a) Isometric view
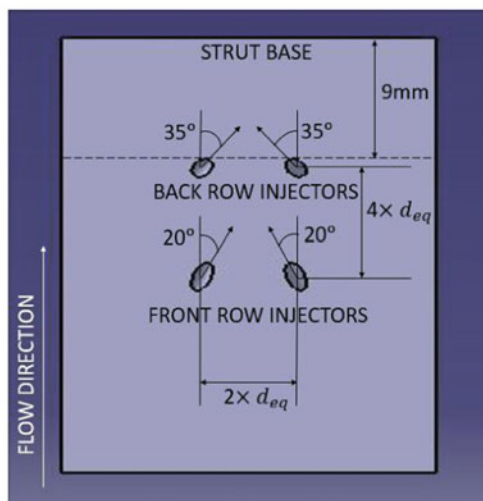
(b) Top view
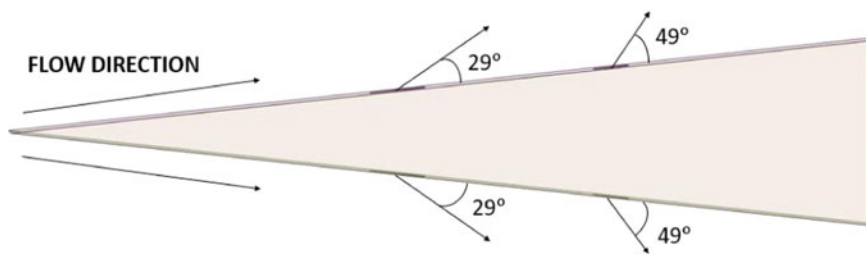
(c) Side view

Fig. 2 Strut geometry with fuel injectors placed 9 mm from base **a** isometric view **b** top view **c** side view

Adaptive Mesh Refinement (AMR) which increased the cell count to 7.7 million. The 3.4 million cell mesh was able to capture the flow field details accurately and used in the analysis.

2.3 Solver Setup

2.3.1 Governing Equations

The numerical analysis in this study was performed using the Ansys Fluent 17.2, which solves the Reynolds Averaged Navier Stokes Equations (RANS) for the flow field. The RANS equations are as follows:

Continuity:

$$\frac{\partial \rho}{\partial t} + \frac{\partial}{\partial x_i}(\rho u_i) = 0 \tag{2}$$

Momentum:

$$\frac{\partial}{\partial t}(\rho u_i) + \frac{\partial}{\partial x_j}(\rho u_i u_j) = -\frac{\partial p}{\partial x_i} + \frac{\partial}{\partial x_j}\left[\mu\left(\frac{\partial u_i}{\partial x_j} + \frac{\partial u_j}{\partial x_i}\right)\right] + \frac{\partial}{\partial x_j}\left(-\rho \overline{u_i' u_j'}\right) \tag{3}$$

Energy:

$$\frac{\partial}{\partial t}(\rho E) + \nabla \cdot (\vec{v}(\rho E + p)) = \nabla \cdot \left(k_{eff}\nabla T - \sum_j h_j \vec{J}_j + \left(\bar{\tau}_{eff} \cdot \vec{v}\right)\right) \tag{4}$$

The fluctuating component is given by:

$$\frac{\partial}{\partial x_j}\left(-\rho \overline{u_i' u_j'}\right) \tag{5}$$

The k-ω SST turbulence model is used to calculate the Reynolds stresses. It is known to be reasonably accurate for a wide class of flows involving adverse pressure gradient and shock induced flow separation. It was also shown to capture species concentration gradients in a subsonic recirculation region behind a step in supersonic flow [13].

Species transport equation:

$$\frac{\partial}{\partial t}(\rho Y_i) + \nabla \cdot (\rho \vec{v} Y_i) = -\nabla \cdot \vec{J_i} + R_i \tag{6}$$

where R_i is net rate of production of species *'i'* by chemical reaction.

The transport of enthalpy due to species diffusion is given by $\nabla \cdot \left[\sum_{i=1}^{n} h_i \vec{J_i} \right]$ and included in the Energy equation.

2.3.2 Boundary Conditions

Air enters the combustor inlet at Mach 2 with a stagnation temperature and pressure of 612 K and 782.45 kPa respectively. Mach 2 corresponds to 732 m/s at 340 K static temperature. The turbulence intensity was set to 5%. The outlet was set as a pressure outlet with non-reflecting boundary condition in lieu of supersonic flow. The strut surface and walls were set as stationary adiabatic walls with no-slip condition. Vertical symmetry was used to model only half of combustor geometry. RANS CFD analysis was performed using k$-\omega$ SST turbulence model and compressibility correction enabled. The flow and turbulence parameters were set to vary as 2nd order upwind to maintain a balance between accuracy and the computational resources required. The Courant number was initialized to a sufficiently low value of 5, which was changed by the solver to maintain convergence.

Hydrogen was injected from all 8 holes, with injection parameters given in Table 1. Three cases were analyzed, two with the location of Aeroramp injectors from strut base varied from 3 to 9 mm and dynamic pressure ratio held constant at q = 1.9. The other case involved changing the dynamic pressure ratio from 1.9 to 3.5, with the location of Aeroramp injectors held constant at 9 mm from strut base. The values of static pressure (P) and Mach number (M) for the freestream in dynamic pressure ratio calculation (Eq. 1) are taken after the oblique shock formed at the strut tip.

Fuel-air mixing in cold flow is the sole focus of this study. Hence, volumetric combustion model used for reactive analysis is disabled in the current work. It must be noted, however, that the results obtained from cold flow analysis will only show a part of the flow physics and mixing involved in the combustor, phenomenon such as dilation encountered with actual reactive flows will change the results observed with cold flow analysis alone. Combustion experiments performed with dual injectors have shown that there would be augmentation of mixing due to "blockage effect", where front row of injectors blocks the flow leading to back injectors, thus allowing the back injectors to achieve better penetration and also resulting in stronger chemical reactions [14, 15]. Hence, further reacting flow analysis should be performed to fully establish the actual flow behaviour occurring in the scramjet combustor.

Table 1 H_2 injection parameters for strut with Aeroramp injection configuration

Location of injectors (from strut base)	Dynamic pressure ratio (q)
3 mm	1.9
9 mm	1.9
9 mm	3.5

3   Results and Discussion

3.1   Mesh Independence and Validation

The gas dynamics of flow past the strut is shown in Fig. 3. Oblique shocks are formed at the strut tip, these shocks reflect toward the centre line after impacting the walls. The shock reflections are not entirely symmetric about the centreline because of the 3° divergence on the upper wall. At the base of the strut, the flow separates leading to the formation of a recirculation region behind the strut, along with expansion fans at the rear edges.
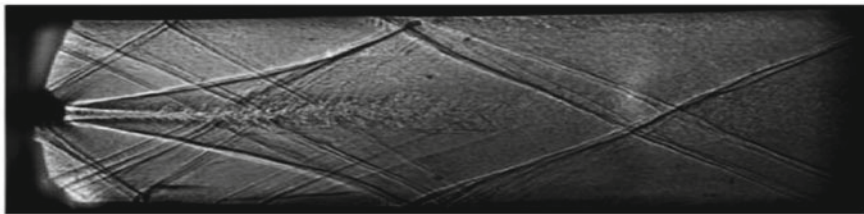
(a) Experimental Schlieren [1]
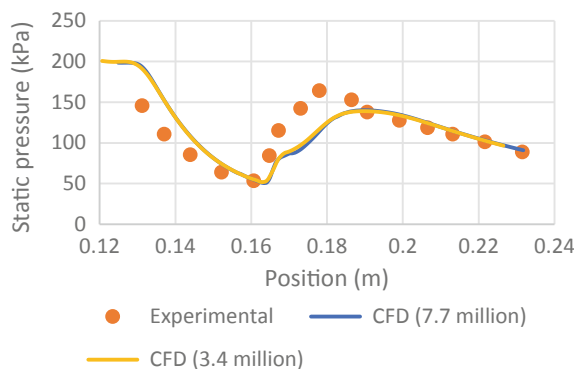
(b) CFD Schlieren

(c) Static pressure along bottom wall of combustor.

Fig. 3   Gas dynamics of flow around strut flame holder without injection **a** Experimental Schlieren [1] **b** CFD Schlieren **c** static pressure along bottom wall of combustor

Two shear layers are formed which separate the recirculation region and the main supersonic flow; they are pushed towards the centre by the expansion fans. As they curve back into the main flow, shock waves are formed. These shock waves reflect against the walls and interact with the boundary layer, which separates at the shock-boundary layer interaction zone due to adverse pressure gradient produced by the shock. A smaller recirculation zone can be seen where the shock reflects off the upper wall due to the 3° divergence angle.

Figure 3 also shows the comparison of the CFD density gradient contours with the experimental schlieren image obtained from [1]. The gas dynamics flow details in the CFD results match well with the schlieren image. The turbulent region behind the strut appears to be smoothened because time averaging was employed in the RANS model. Lower wall static pressure variation obtained downstream of the strut base from [1] and the CFD results were compared as shown in Fig. 3c. The initial decrease in pressure can be attributed to the expansion fan at the strut base. Later, the pressure increases due to the shock wave originating at the shear layer reflecting off the lower wall. The CFD results are in reasonable agreement with the experimental static pressure decrease due to the expansion fan, the minima being captured well in CFD. However, it predicts a weaker oblique shock and hence a lower pressure rise compared to the experiment.

The data for velocity validation was obtained from [1]. Here, three velocity profiles at distances of 11 mm, 58 mm and 166 mm from the base of strut and on symmetry plane were plotted against experimental values (Fig. 4). The strut length was 32 mm. A velocity deficit is observed in the recirculation region, which gradually reduces as we move away from the strut. In general, the velocity profiles between CFD and experiment are in good agreement. At x = 11 mm, the maximum velocity difference in recirculation region is 16%, while at other locations it is within 7%.

Both the 3.4 and 7.7 million cell mesh results are surprisingly close to each other, except x = 11 mm location, where the 3.4 million mesh data is closer to the experimental results than the 7.7 million mesh data. The wall static pressure variation also overlaps for the two meshes (Fig. 3c). Hence, the 3.4 million mesh was used in subsequent analysis.

3.2 Strut with Aeroramp Injector

3.2.1 Gas Dynamics of Flow Field

The flow field that results due to injection into supersonic cross-stream involves gas dynamics details that play a significant role in the overall mixing of fuel with air. In order to understand these details, Schlieren images are taken, giving the side view of strut and associated flow field for the three injection cases (Fig. 5), along with streamlines image giving the isometric view of fuel injected from the Aeroramp holes (Fig. 6).
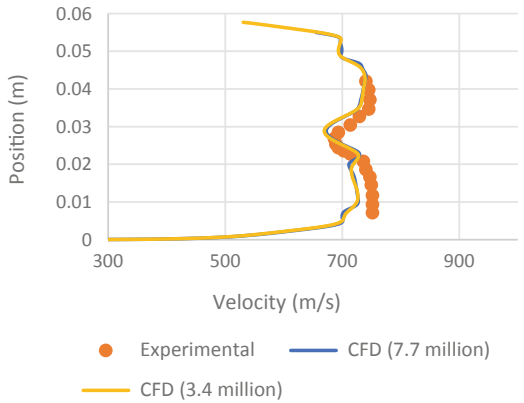
Fig. 4 Velocity profiles at
a 11 mm **b** 58 mm **c** 166 mm
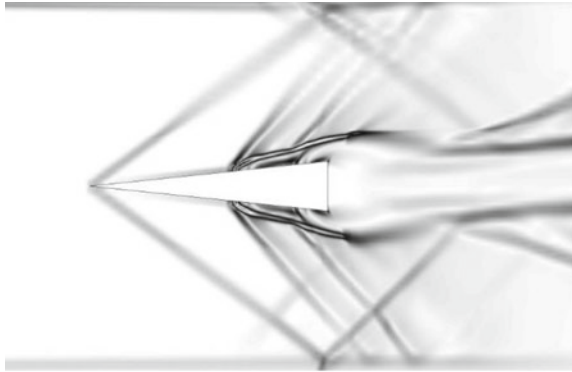behind the strut on the
symmetry plane
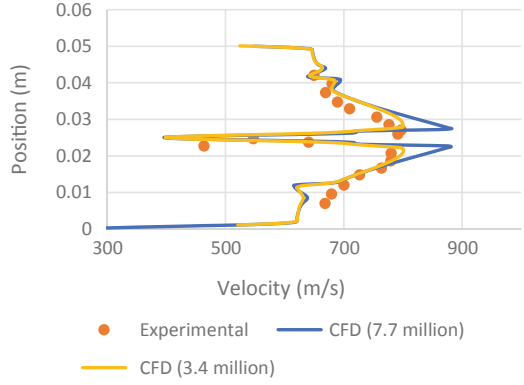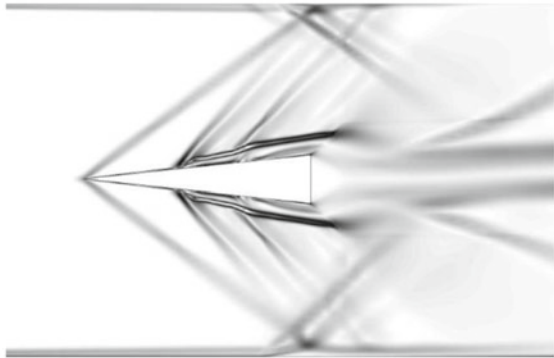
(a) Velocity profile at 11mm
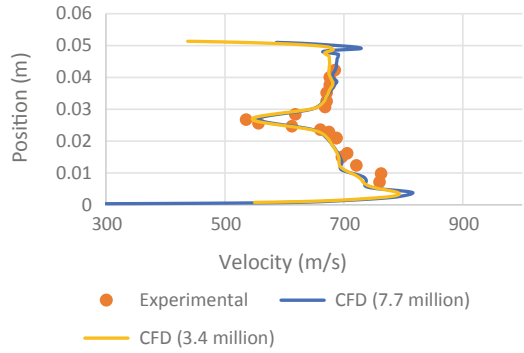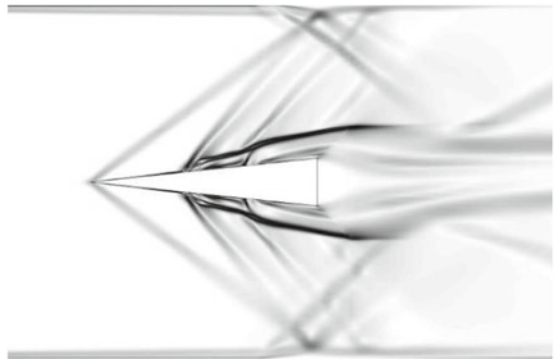
(b) Velocity profile at 58mm

(c) Velocity profile at 166mm

Fig. 5 CFD Schlieren images for various fuel injection configurations from strut upper and lower surfaces **a** 3 mm, q = 1.9 **b** 9 mm, q = 1.9 **c** 9 mm, q = 3.5

(a) 3mm, q = 1.9
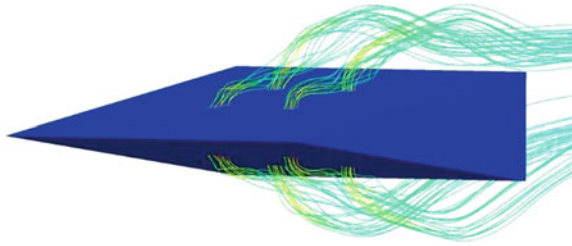
(b) 9mm, q = 1.9

(c) 9mm, q = 3.5

Fig. 6 Streamlines of H$_2$
injection for 9 mm, q = 3.5

The CFD Schlieren images are given in Fig. 5 for strut with Aeroramp injectors. Schlieren is the first derivative of the density in the flow field. Hence the gradient of density is shown in these images in a vertical plane cutting through the fuel injectors. The region around the strut is shown to explain the effects of injection and the flow details associated with it. The region further downstream has some differences with that seen without injection. The reflected shocks originating at strut tip are at greater angles than that seen with just the strut, they get strengthened from the bow shocks emanating due to the injector jets. However, the shocks originating at the shear layer are weaker in the case with injection; their strength is controlled by the weaker expansion fan due to lower Mach number flow approaching the strut base.

The bow shocks ahead of the fuel jets are visible, with the bow shock formed as a result of front injectors stronger than the rear. This shields the rear jets and "blocks" the main flow to some extent, allowing better penetration of the rear jets into the core flow. The strength of these bow shocks is directly related to dynamic pressure ratio; higher the dynamic pressure ratio of injection, stronger the bow shocks associated with each injector. The fuel jets after injection undergo expansion due to the pressure gradient and subsequently lead to a Mach disk downstream. When the injector holes are 9 mm from the base of strut, for q = 3.5 (Fig. 5c), the Mach number at the strut base is lower compared to q = 1.9 (Fig. 5b) because of stronger bow shocks. This results in a weaker expansion fan and less turning of flow downstream of the strut base. Hence, the recirculation zone behind the strut is larger for q = 3.5. It has implications for fuel-air mixing, as discussed later.

The streamlines of hydrogen jets are shown for 9 mm, q = 3.5 in Fig. 6, with an isometric view encompassing the recirculation region at the strut base. The streamlines give the direction of fuel jets after injection, the effect of the Aeroramp can be seen in these images. The "blockage effect" of the front row of injectors allows the back row to bump up the fuel stream deeper into the core flow. As a result, the penetration of the fuel into the freestream is improved in the near field. At the strut base, the expansion fan forces the fuel vortices to turn back into the recirculation region, hence improving its mixing with air.

An important constraint in the development of combustor is the overall stagnation pressure loss incurred from inlet to exit. The flame holder and the fuel injection technique play a crucial role in this context. The stagnation pressure loss for various cases is given in Table 2.

Table 2 Overall stagnation pressure loss (%) for various cases

| Case	Stagnation pressure loss (%)
Only strut (without injection)	21
3 mm, q = 1.9	22.7
9 mm, q = 1.9	21
9 mm, q = 3.5	20.6

Since the number of fuel injector holes is less, the injection process causes only a minor increase in mass-averaged stagnation pressure loss across the combustor; the maximum increase is 1.7% among the aero-ramp cases compared to the strut only case. An apparent anomaly observed in the table is that the loss is 0.4% lesser for the 9 mm, q = 3.5 case than loss without injection. As discussed earlier, the bow shocks due to fuel injection increase the losses, while the weaker shocks originating at the shear layer reduce the losses. For the case under discussion, the net effect of these two shock structures is a reduction in overall loss.

3.2.2 Equivalence Ratio Variation

The Equivalence ratio contours in Fig. 7 give a good picture of the mixing process from combustion point of view. Although combustion runs are not performed here, the equivalence ratio depicts what part of the fuel-air mixture in a plane is combustible. The outer black line in each image corresponds to Lower Flammability Limit (LFL) and the inner black line corresponds to Upper Flammability Limit (UFL). For the given airflow conditions, these values of LFL and UFL correspond to equivalence ratios of 0.1 and 2.1 respectively. Only the region between these limits is combustible; the region within the UFL line is very fuel rich and not combustible and the region outside the LFL line is very fuel lean and hence not combustible. This combustible region is compared among the three cases and along four planes downstream of strut base in the recirculation region, as most of the mixing occurs here.

Figure 7 shows the equivalence ratio contours for the three injection cases at four locations downstream of the strut base. The distance x is normalized by strut length L. At $x/L = 0.5$ given by Fig. 7a, for 3 mm, q = 1.9, the Aeroramp vortices are forced to turn by a sharp angle towards the recirculation zone due to the expansion fan at the strut base. Thus, there is some interaction of the Aeroramp vortices with the strut wake vortex. For the 9 mm, q = 1.9 case, the strut wake vortices are shorter due to the stronger expansion fan as discussed earlier. Hence, in contrast to the 3 mm case, the Aeroramp vortices have a more limited interaction with the strut wake vortices. In the 9 mm, q = 3.5 case, the recirculation vortex is larger, resulting in a stronger interaction and enhanced mixing with the Aeroramp vortices. There is also higher penetration in the vertical and lateral directions in this case compared to the previous two cases.

At $x/L = 1$ given by Fig. 7b, for 3 mm, q = 1.9, the orientation of these vortices is changed as they are pulled inwards by the significantly stronger recirculation zone

(a) x/L = 0.5
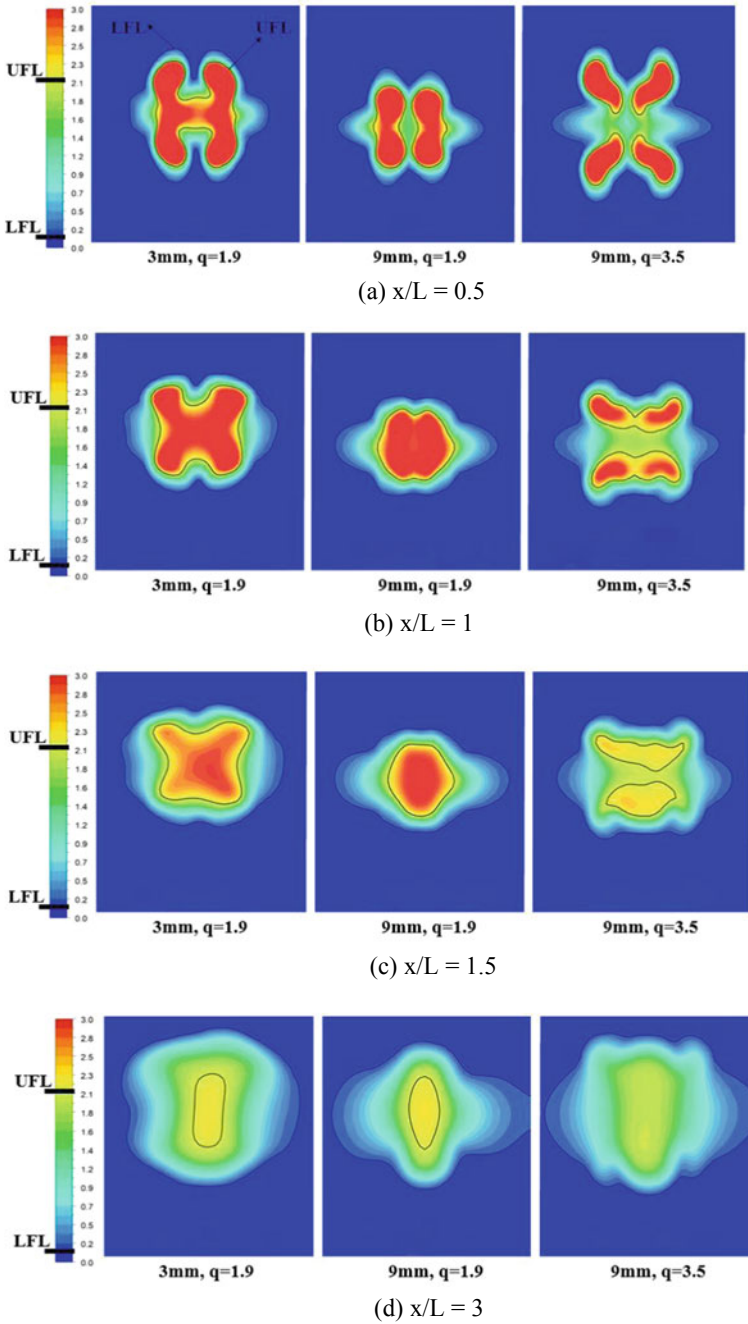
(b) x/L = 1

(c) x/L = 1.5

(d) x/L = 3

Fig. 7 Equivalence ratio contours for various fuel injection configurations at **a** x/L = 0.5 **b** x/L = 1 **c** x/L = 1.5 **d** x/L = 3

vortex. The orientation of the jet vortices is maintained for the 9 mm, q = 1.9 due to limited interaction with the recirculation vortex, hence causing a lateral bulge in the equivalence ratio contours. In the 9 mm, q = 3.5 case, the interaction is so significant that the Aeroramp vortices are flattened and each vortex begins interacting with the vortex adjacent to it in the lateral direction.

At $x/L = 1.5$ given by Fig. 7c, for 3 mm, q = 1.9, the Aeroramp vortices have merged together in an 'X' like pattern and for 9 mm, q = 1.9, all the Aeroramp vortices have merged into a single fuel rich blob. For the 9 mm, q = 3.5 case, the interaction with the strut wake vortex and adjacent vortices have resulted in the fuel richness dropping more prominently (from bright red to light yellow) than that seen in the other two cases.

At $x/L = 3$ given by Fig. 7d, we can see that the fuel richness has dropped rapidly to values below the UFL in 3 mm, q = 1.9 and 9 mm, q = 1.9 cases. There is still a central fuel rich region in these two cases that is not combustible. However, in the 9 mm, q = 3.5 case, there is no UFL as the mixing of fuel and air has been so extensive that the entire region within the LFL line is combustible.

This concludes that the best-case scenario is injecting at a higher dynamic pressure ratio (q = 3.5) and away from the strut base (9 mm). The fuel penetrates the incoming air better in both lateral and vertical directions and stays away from the injection surface. Fuel-air mixing is also enhanced around and behind the strut. The combustible area is higher at all locations for this case compared to the other two cases. To add to these advantages, the overall stagnation pressure loss is also lower for the 9 mm, q = 3.5 case than in the other two cases.

In Fig. 7, the region within the UFL line is bright red, signifying a very fuel rich mixture. Although the maximum equivalence ratio for these contours has been truncated at 3, the equivalence ratios in these fuel rich regions go well beyond 3.

The graph in Fig. 8 gives the maximum equivalence ratio variation from the strut base up to $x/L = 4$. The 9 mm location cases show lower maximum equivalence ratio compared to 3 mm case, since the Aeroramp vortices get more distance along the strut length to mix with air. While comparing the 9 mm, q = 1.9 and 9 mm, q = 3.5 cases, an interesting observation is that although more fuel is injected for the 9 mm, q = 3.5 case at higher dynamic pressure ratio, enhanced mixing with the larger strut wake vortex ensures that the local maximum equivalence ratio is lower than the 9 mm, q = 1.9 case.

4 Conclusion

The current study explores a novel strut-based fuel injection scheme for a scramjet combustor, incorporating an aerodynamic ramp fuel injector on the upper and lower strut surfaces. As the first step, the gas dynamics of flow past the strut using RANS CFD analysis were validated with DLR experimental data available in literature. The velocity profiles behind the strut, lower wall static pressure and density gradients agreed well with experiment.
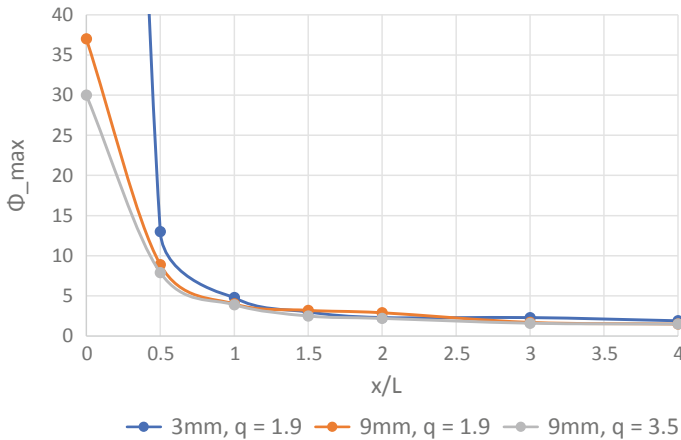
Fig. 8 Maximum equivalence ratio variation as a function of distance behind the strut for various fuel injection configurations

The Aeroramp injectors were incorporated on the strut surface to increase the lateral fuel penetration into the flow and improve mixing by Aeroramp vortices in the near field up to strut base. These vortices subsequently entrain into the larger strut wake recirculation vortex and further enhance fuel-air mixing.

The location of Aeroramp injectors with respect to strut base (3 mm, 9 mm) and dynamic pressure ratio (q = 1.9, 3.5) were varied. The fuel injected was hydrogen, only non-reacting flow runs were performed. Numerical schlieren, streamlines and equivalence ratio contours in various transverse planes behind the strut were obtained. The results indicate that it is beneficial to inject fuel away from the strut base and at a higher dynamic pressure ratio to achieve better fuel-air mixing and lower equivalence ratios downstream of the strut, which is more amenable to combustion. Fuel-air mixing is governed by the interaction of Aeroramp vortices with the larger strut wake recirculation vortex; the strength of expansion fan at strut base plays a key role in facilitating this interaction.

References

1. Genin F, Menon S (2010) Simulation of turbulent mixing behind a strut injector in supersonic flow. AIAA J 48(3):526–539
2. Berglund M, Fureby C (2007) LES of supersonic combustion in a scramjet engine model. Proc Combust Inst 31:2497–2504
3. Changmin Cao, Taohong Ye, Majie Zhao (2015) Large eddy simulation of hydrogen/air scramjet combustion using tabulated thermo-chemistry approach. Chin J Aeronaut 28(5):1316–1327
4. Fuller RP, Wu PK, Nejad AS, Schetz JA (1998) Comparison of physical and aerodynamic ramps as fuel injectors in supersonic flow. J Propul Power 14(2):135–145
5. Segal C (2009) The scramjet engine: processes and characteristics. Cambridge University Press

6. Cox SK, Fuller RP, Schetz JA, Walters RW (1994) Vortical interactions generated by an injector array to enhance mixing in supersonic flow. In: AIAA Paper, 94-0708

7. Jacobsen LS, Gallimore SD, Schetz JA, O'Brien WF, Goss LP (2003) Improved aerodynamic-ramp injector in supersonic flow. J Propul Power 19(4):663–673

8. Jacobsen LS, Schetz JA, Ng WF (2000) Flowfield near a mulitiport injector array in a supersonic flow. J Propul Power 16(2):216–226

9. Jacobsen LS, Gallimore SD, Schetz JA, O'Brien WF (2003) Integration of an aeroramp injector/plasma igniter for hydrocarbon scramjets. J Propul Power 19(2):170–182

10. Bonanos AM, Schetz JA, O'Brien WF (2008) Dual-mode combustion experiments with an integrated aeroramp-injector/plasma-torch igniter. J Propul Power 24(2):267–273

11. Baoxi W, Chen B, Yan M, Shi X, Zhang Y, Xu Xu (2012) Operational sensitivities of an integrated aerodynamic ramp injector/gas portfire flame holder in a supersonic combustor. Acta Astronaut 81:102–110

12. Chen B, Xu Xu, Baoxi W, Zhang Y (2017) Numerical simulations of turbulent flows in aeroramp injector/gas-pilot flame scramjet. Chin J Aeronaut 30(4):1373–1390

13. Thakur A, Sinha A, Roy AS, Ghosh D, Ali MS, Poptani S (2017) CFD analysis and validation of mixing and combustion behind a step flame holder in supersonic flow. In: 1st National aerospace propulsion conference, NAPC-2017-024

14. Lee SH (2006) Characteristics of dual transverse injection in scramjet combustor, Part 2: combustion. J Propul Power 22(5):1020–1026

15. Lee SH (2006) Characteristics of dual transverse injection in scramjet combustor, Part 1: mixing. J Propul Power 22(5):1012–1019